Numerical Study of the Entrance Flow and its Transition of a Circular Pipe

By

H. KANDA* and K. OSHIMA

(January 27, 1986)

Summary: Two-dimensional, time-dependent computational scheme has been devised for determining the flow development and the corresponding pressure drop in the entrance region of a circular pipe at the Reynolds numbers based on the pipe diameter of 10, 100, 2000, and 10000. An iterative, stream function-vorticity formulation was applied, utilizing a mesh system in which the axial grid size is nearly proportional to the Reynolds number. The velocity field, the pressure drop, and the convective and the viscous terms are compared with the experimental results and also with the previous analysis. Moreover, the effects of the Reynolds number and the superposed disturbances on the transition from laminar to turbulent flow were numerically simulated.

§I. INTRODUCTION

Since G. Hagen (1839) and J. Poiseuille (1841), the case of laminar and turbulent flow through circular pipes has been investigated very thoroughly in the past because of its great practical importance. Moreover, the results are important not only for pipe flow, but also for the contribution to the extension of our fundamental knowledge of turbulent flow in general. The origin of turbulence and the accompanying transition from laminar to turbulent flow has never been still unsolved.

When fluid particles enter into a circular pipe from a large container, the velocity distribution in the cross-section varies with the distance from the initial inlet. In sections close to the inlet the velocity distribution is nearly uniform. Further downstream the velocity distribution changes, owing to the influence of friction, until a fully developed velocity profile is attained at a given distance, which is called the entrance length. The dimensionless entrance length, which is denoted as Lep, is defined as the entrance length divided by the diameter of a pipe and the Reynolds number: Lep=zep/(D*Re), where zep is the entrance length, D is the diameter of a pipe and subscript p means 'parabolic'. The dimensionless entrance length Lep=zep/(D*Re) is supposed to be within the range of 0.02875 [*1*], 0.058 [*2*], 0.072 [*3*], and 0.1 at most. Moreover, it has been experimentally known to be proportional to the Reynolds number [*4*].

The laminar entrance region in turbulent flow is considerably shorter than that in laminar flow. According to the measurement performed by 0. Reynolds its length is about 20 to 30 diameters [*5*], 50 to 100 by H. Kirsten [*6*], below 17.5 to 35 by M. Arakawa [*7*], and is observed below 100 by K. Oshima [*8*]. This entrance length is denoted as Let in the dimensionless form: Let=zet/(D*Re), where t means 'transition'. When the entrance length of 100 diameters is divided by the minimum critical Reynolds

* Science Institute, IBM Japan, Ltd.

number 2300, Lep is 0.0435.

It can be stated that the laminar flow which is formed close to the entrance of the pipe is unstable and becomes turulent owing to very small unavoidable disturbances. The numerical value of the critical Reynolds number at which the transition starts can be stated to depend very strongly on the conditinons which prevail in the entrance region as well as in the approach to it.

To sum up, the transition from laminar to turbulent flow is supposed to occur only in the entrance region, before Lep.

In this paper, the development of the time-dependent flow of an incompressible Newtonian fluid in the entrance region of a circular pipe is analyzed by the numerical solution of the complete two-dimensional equations of motion.

§II. Computational Scheme

2.1 Mesh system and basic equations

Fig. 1 shows the z and r coordinates and the mesh system formed by the orthogonal lines separated by a constant space increment Δz on the z-axis and Δr on the r-axis. The basic equations are written by the finite-discrete formulation on the discrete points formed by the mesh system.

Because of the azimuthal symmetry of a circular pipe, it is utilized the rectangular grid system composed of the region $0 \leq z \leq z0$ and $0 \leq r \leq 0.5$, where z and r are the axial and radial coordinates, respectively, and are made dimensionless by being divided by the diameter of a circular pipe. The axial point i takes an integer value between 1 and 10 and the radial point j is between 1 and J0.

The number of the mesh points becomes I0*J0. In order to obtain the accurate numerical solutions, it is necessary to make the number of mesh points, I0 and J0, larger. On the other hand, there are some severe limitations on a computer main storage size and computational power.

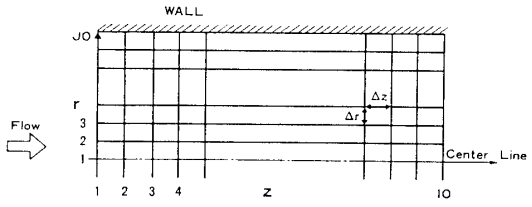

Fig. 1. Mesh System.

For the entrance region described above we consider the 2-dimensional, unsteady flow of an incompressible Newtonian fluid with constant viscosity and density. We neglect gravity and external forces. Consequently, the dimensionless forms of the stream function-vorticity equation and the Poisson equation are written in the cylindrical coordinates, Stream function-Vorticity equation:

$$\frac{\partial \omega}{\partial t} - \frac{1}{r}\frac{\partial \psi}{\partial z}\cdot\frac{\partial \omega}{\partial r} + \frac{1}{r}\frac{\partial \psi}{\partial r}\cdot\frac{\partial \omega}{\partial z} + \frac{\omega}{r^2}\frac{\partial \psi}{\partial z} = \frac{1}{\mathrm{Re}}\left\{\frac{\partial}{\partial r}\left(\frac{1}{r}\frac{\partial}{\partial r}(r\omega)\right) + \frac{\partial^2 \omega}{\partial z^2}\right\} \qquad (1)$$

Poisson equation:

$$-\omega=\frac{\partial}{\partial r}\left(\frac{1}{r}\frac{\partial \psi}{\partial r}\right)+\frac{\partial^2}{\partial z^2}\left(\frac{\psi}{r}\right) \tag{2}$$

Table 1 gives the initial and boundary conditions, where I1=I0–1 and I2=I0–2. The whole fluid particles start moving downstream with uniform velocity in a pipe at the initial time. The no-slip boundary condition is on the wall and any vorticity does not exist at the inlet and on the center line of a circular pipe. Moreover, the outlet condition is given by extrapolation.

The axial and radial velocity, u and v, are calculated from the derivatives of stream function in the general method:

$$u=\frac{1}{r}\frac{\partial \psi}{\partial r} \tag{3}$$

$$v=-\frac{1}{r}\frac{\partial \psi}{\partial z} \tag{4}$$

The pressure drop within the region is writtin in the Poisson form.

$$\frac{\partial}{\partial r}\left(r\frac{\partial p}{\partial r}\right)+\frac{\partial}{\partial z}\left(r\frac{\partial p}{\partial z}\right)=r\left\{\left(\frac{\partial v}{\partial r}\right)^2+2\frac{\partial u}{\partial r}\cdot\frac{\partial v}{\partial z}+\left(\frac{\partial u}{\partial z}\right)^2\right\}+\frac{v^2}{r} \tag{5}$$

And the derivative of the pressure on the wall is as follows in the normal direction by C. E. Pearson [9],

$$\frac{\partial p}{\partial s}=-\frac{1}{\mathrm{Re}}\frac{\partial \omega}{\partial n} \tag{6}$$

where S and n are the tangential and normal directions, respectvely.

Table 1. Initial and Boundary Conditions

Conditions	Stream Function	Vorticity
Initial	$\frac{1}{2}\left(\frac{J-1}{Jo-1}\right)^2$	0
Boundary		
Inlet	$\frac{1}{2}\left(\frac{J-1}{Jo-1}\right)^2$	0
Wall	$\frac{1}{2}$	$2\frac{\psi(1,Jo)-\psi(1,J1)}{\Delta r^2}$
Center	0	0
Outlet	$2\psi(I1,J)-\psi(I2,J)$	$2\omega(I1,J)-\omega(I2,J)$

2.2 Values of mesh system and time increment

As the Reynolds number increases, the entrance length becomes longer and we need more axial grid points if the aspect ratio of Δz to Δr is same for all Reynolds numbers.

We suppose the value of Lep is nearly constant regardless of the Reynolds number and divide the range zep by the same axial grid number, so that the dimensionless axial grid length is same for all Reynolds numbers. Consequently, the ratio of Δz to Δr, which is denoted as DZR, becomes proportional to the Reynolds number.

It depends very strongly on the time increment whether time-dependent computational schemes may converge or not. When the flow field is computed time-dependently, at least 2000 time steps are needed for each case.

The smaller the time increment is, the better the convergence of computational numerical calculation is obtained. The time increment was derived from Equation [7].

$$\Delta t = \frac{A}{4\left(\frac{1}{\Delta z^2}+\frac{1}{\Delta r^2}\right)+\frac{1}{\Delta z}+\frac{1}{\Delta r}} \tag{7}$$

where A is a mere coefficient for the convergence. If the results of the numerical computation becomes divergent, A must be made smaller than the current value for the convergence of the computation. If the scheme is in a convergent state until the steady state is reached, A can be made larger than the current value for the computational performance.

Table 2 gives the values of the time increment and the number of time step at which the steady state is obtained, with respect to the Reynolds number.

As the ratio *DZR* increases largely with the Reynolds number, the derivatives with respect to z decreases and become ineffective in the basic equations. However, in the *DZR* range of 1 and 500, the derivatives with respect to z were meaningfully effective owing to double precision variables of IBM VS FORTRAN of 14 hexadecimal digits.

2.3 Calculation steps

Both of the stream function and the pressure are calculated by the Gauss-Seidel iterative method. The variable at $(m+1)$ iteration is calculated by using the values of the present iteration $(m+1)$ which have just been computed. The number of time step n

Table 2.

Re	IO	JO	Δz/Δr	Δt	N(xΔt)
10	100	21	1	0.00278	2000
100	100	21	10	0.02621	8000
2000	150	21	100	0.04762	8000
10000	150	21	500	0.09901	20000

takes an integer between 1 (initial time) and N (steady state) in Table 2.

The iterative method of the numerical solution is summarized as follows:

$$\omega^n = f_1(\psi^n) \tag{8}$$

$$\omega^{n+1} = \omega^n + \Delta t \cdot f_2(\psi^n, \omega^n) \tag{9}$$

$$\tilde{\psi}^{n+1'}_{m+1} = f_3(\tilde{\psi}^{n+1}_{m+1}, \tilde{\psi}^{n+1}_{m}, \omega^{n+1}) \tag{10}$$

$$\tilde{\omega}^{n+1} = f_1(\tilde{\psi}^{n+1}_{m+1}) \tag{11}$$

$$|\omega^{n+1} - \tilde{\omega}^{n+1}| < \varepsilon \tag{12}$$

1. Assume initial values for ψ throughout the interior of the region and calculate initial values of ω by using Equation (8).
2. Calculate new real values of ω at $(n+1)$ time step by using Equation. (9).
3. Calculate provisional values of $\tilde{\psi}$ at $(n+1)$ time step by using the Gauss-Seidel method and Equation (10).
4. Calculate provisional values of $\tilde{\omega}$ from provisional values of $\tilde{\psi}$ by using Equation (11).
5. Compare provisional values of $\tilde{\omega}$ with real values of ω at $(n+1)$ time step for the whole interior of the region and confirm provisional $\tilde{\omega}$ to see if the convergent criteria are satisfied, by using Equation (12).
6. Repeat steps 3, 4, and 5 until the convergent criteria are satisfied.
7. Calculate velocities from the stream function at $(n+1)$ time step by Eqs. (3) and (4).
8. Calculate pressure drop at $(n+1)$ time step by using the Gauss-Seidel method and Equation (5), within the interior of the region.
9. Calculate pressure drop on the wall by using Equation (6).
10. Repeat for next time step.

§III. Numerical Simulation

3.1 Aspect ratio of space increments $\Delta z/\Delta r$ (DZR)

In this study, the values of the space increments in Table 2 are used. According to the Reynolds number the ratios are selected from 1 to 500. In order to confirm the accuracy of the computational results, the velocity distributions at Reynolds number of 2000 are calculated and compared with one another in three cases of DZR=10, 50, and 100. As the axial grid number I0 remains same, the computed region, which the computational mesh system covers, decreases with smaller DZR. Therefore, the maximum dimensionless computed length is 0.018 in the case of DZR=I0. In Figs. 2–4 ● and ▲ show the results at z*=0.01 and 0.05, respectively, where z* is the dimensionless distance (z*=z/(D*Re)) from the inlet.

They agree very well with one another.

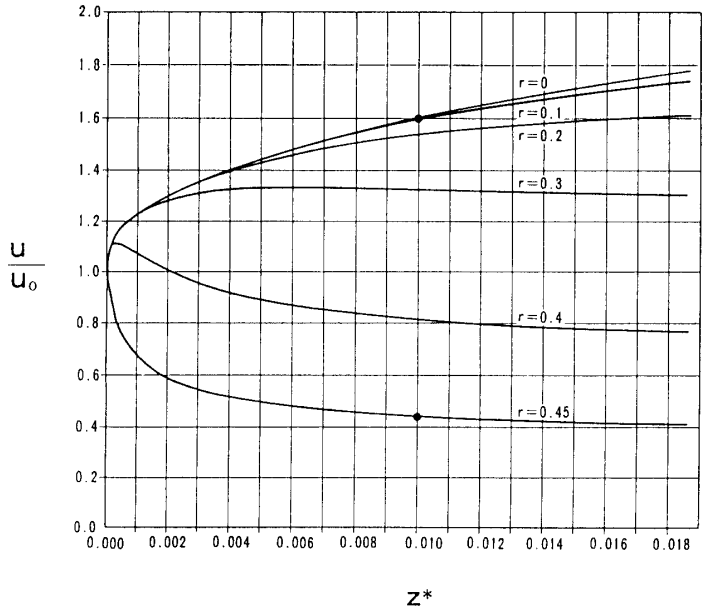

Fig. 2. Velocity Distribution, Re=2000, dz/dr=10.

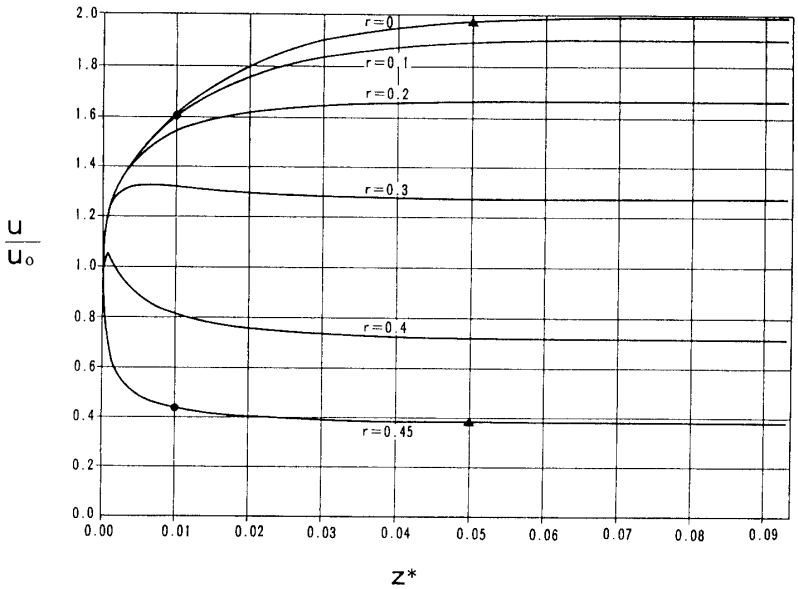

Fig. 3. Velocity Distribution, Re=2000, dz/dr=50.

3.2 Velocity profile and pressure drop

The results are presented for the numerical solution of the comlete, time-dependent equations of motion for four different Reynolds numbers 10, 100, 2000, and 10000. If the number of time step reaches to the value N in Table 2, the flow field can be assumed to be in a steady state because variables at N time step are almost precisely the same as those at (N+1) time step. Figs. 5–8 show the results for the velocity distribution in a steady state. At Reynolds number of 10, in the central $0<r<0.4$ and $z^*<0.05$ region, the axial dimensionless velocities are fairly smaller than those of Reynolds numbers 100, 2000, and 10000. In other words the flow field at Reynolds number 10 develops more

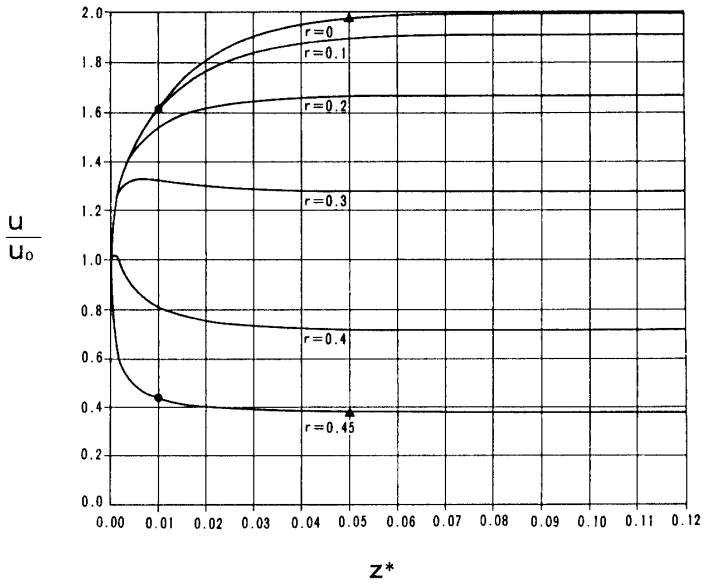

Fig. 4. Velocity Distribution, Re=2000, dz/dr=100.

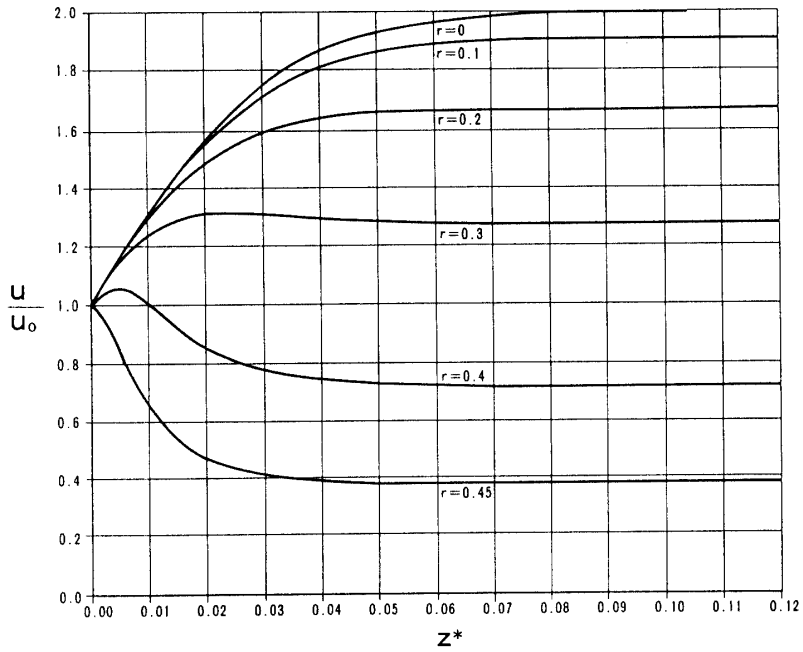

Fig. 5. Velocity Distribution, Re=10, steady state.

slowly than at Reynolds numbers above 100 in the entrance region. For instance, in the case of z*=0.01 and r=0, the axial dimensionless velocity u/u0 is 1.3032 at Re=10; 1.6289 at Re=100, 1.6191 at Re=2000 and 1.6191 at Re=10000. In the case of z*= 0.05 and r=0, u/u0 is 1.9302 at Re=10; 1.9735 at Re=100, 1.9732 at Re=2000 and 1.9733 at Re=10000. However, the flow field in the entrance region develolps completely fully near z*=0.1 and far downstream, that is, the velocity distribution after z*=0.1 is same for all the Reynolds numbers. At the center line r=0, u/u0 is 1.9977 (99.89% of fully developed value) at Re=10; 1.9988 (99.94%) at Re=100, 1.9929

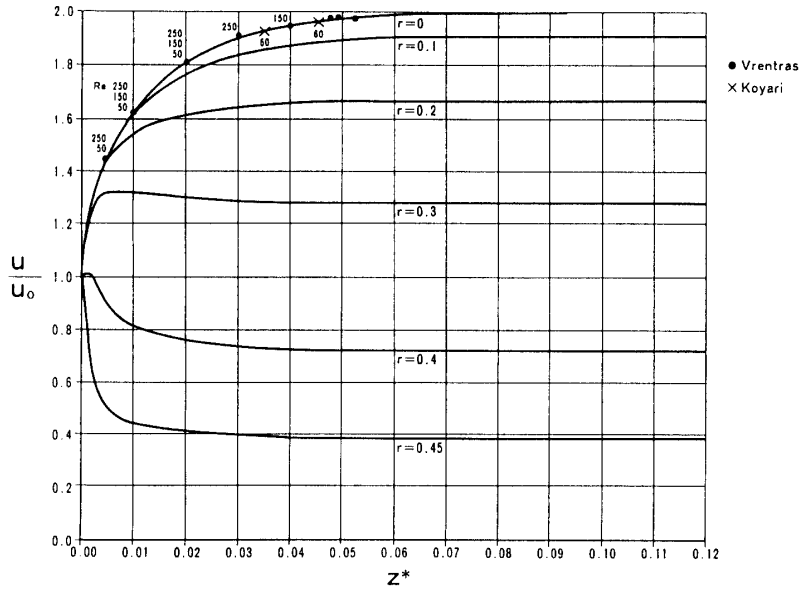

Fig. 6. Velocity Distribution, Re=100, steady state.

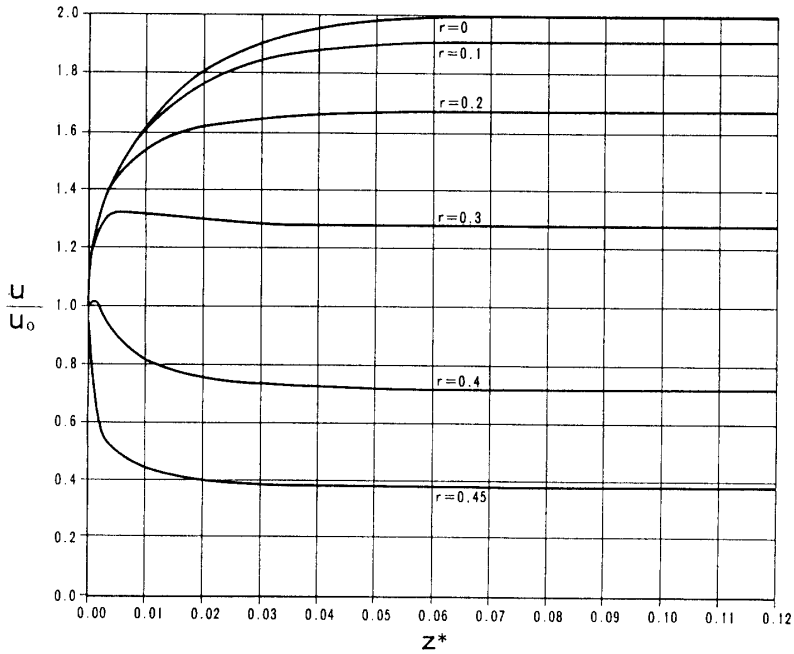

Fig. 7. Velocity Distribution, Re=2000, steady state.

(99.65%) at Re=2000 and 1.9846 (99.23%) at Re=10000. Figs. 9–12 represent the results for the numerical simulation of the pressure drop on the wall in the entrance region. At Reynolds number 10 there are strong vorticities on the wall just after the inlet, and fairly large reverse pressure drop appears. At Reynolds numbers above 100, the pressure drop is uniform in cross section and increases in the almost same degree regardless of the Reynolds number. At Reynolds numbers of 10 and 100, the flow field develops almost fully over $100*\Delta t$ time step since the trends of the computational results of the pressure drop are nearly same in Figs. 9–10.

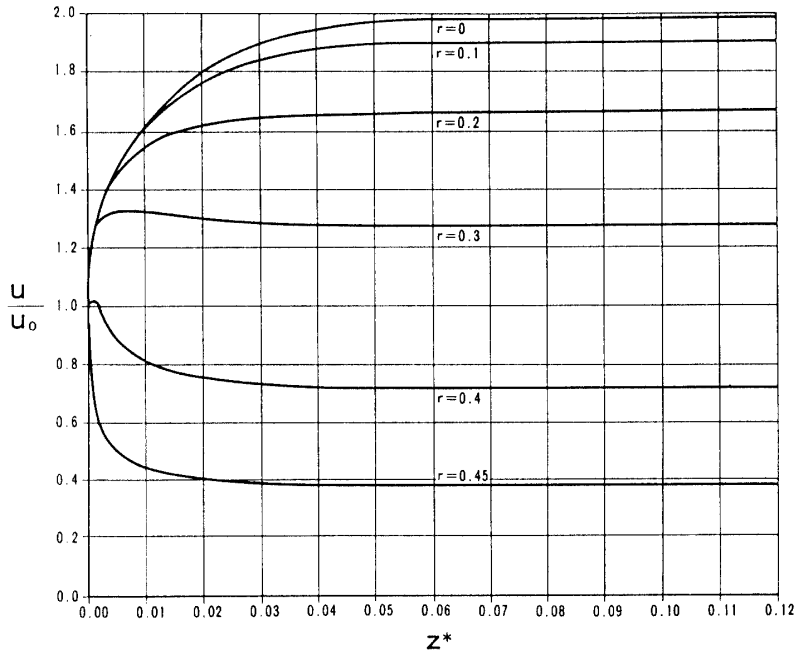

Fig. 8. Velocity Distribution, Re=10000, steady state.

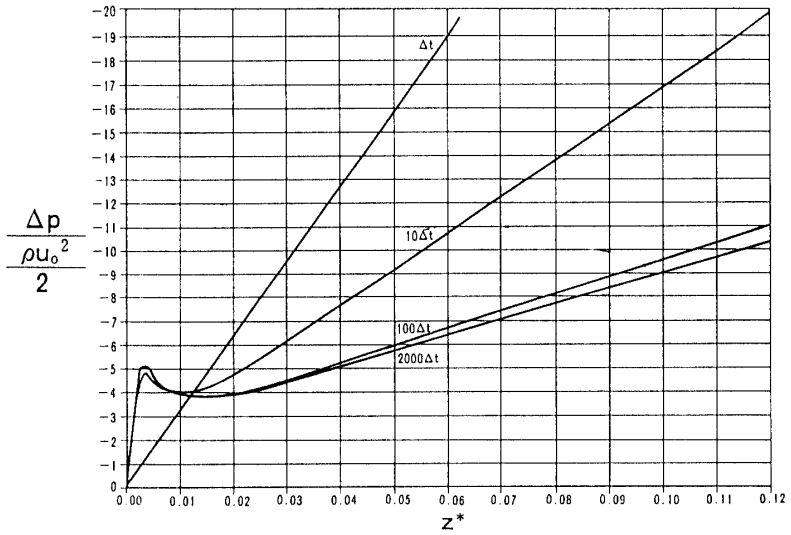

Fig. 9. Pressure Drop, Re=10, on wall.

3.3 Comparison with experimental data and prior analyses

So far various approximate analytical solutions have been devised in order to provide information relating to the flow development and the pressure drop in a circular pipe and a lot of experiments have been made too. Without experimental analyses there have been few analyses for higher Reynolds numbers more than 1000. Therefore, we compare with the results at Reynolds number of 100.

Comparison of velocity: In Fig. 6 ● and × are the results of the numerical solution on the center line by J. S. Vrentas [*10*] and Y. Koyari [*11*], respectively. J. S. Vrentas calculated in the range of Reynolds numbers based on the pipe diameter of 0, 1, 50, 150,

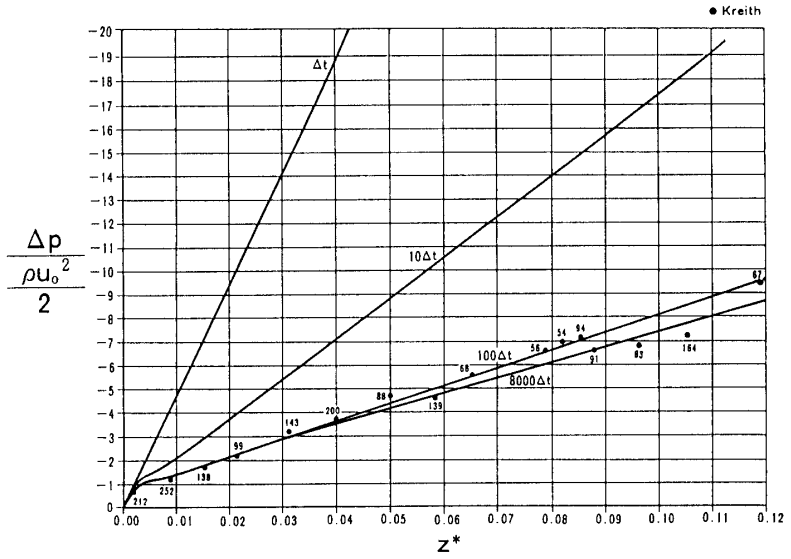

Fig. 10. Pressure Drop, Re=100, on wall.

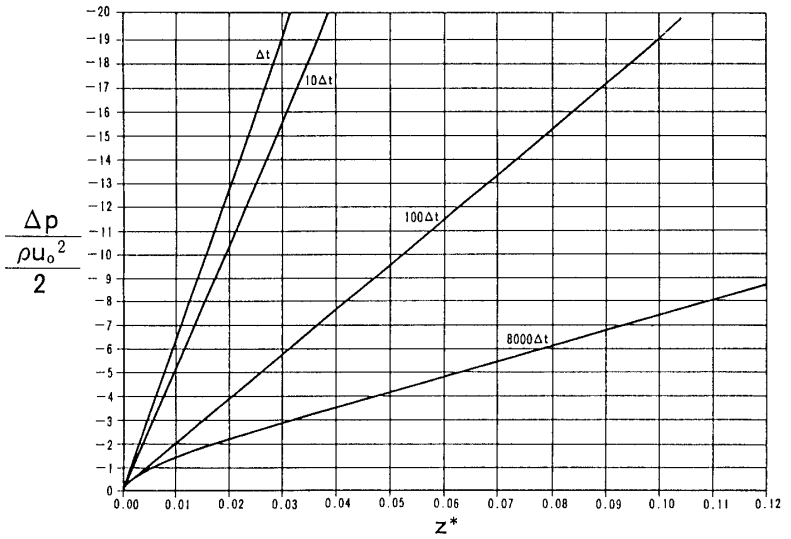

Fig. 11. Pressure Drop, Re=2000, on wall.

and 250. Y. Koyari calculated at Reynolds number of 60. The results show that the axial velocity distributions and the velocity development are nearly same for Reynolds numbers more than 50. Table 3 shows the some results of the numerical solution. According to Table 3 we can say in general that the dimensionless entrance length of 98% of fully developed value is about 0.045 and that of 99% is nearly 0.055 for Reynolds numbers above 50. Moreover, that of 100% may well be determined to be 0.1.

Comparison of pressure drop: In the entrance region of a pipe, it is necessary to have a larger pressure drop per unit length than is required in te fully developed flow, since a part of this drop is utilized for accelerating the central core and consequently for increasing the kinetic energy of the flow. The excess pressure drop is the function of both of the entrance distance from the inlet and the Reynolds number.

Fig. 10 shows the comparison of the experimental data by F. Kreith [*12*] and the

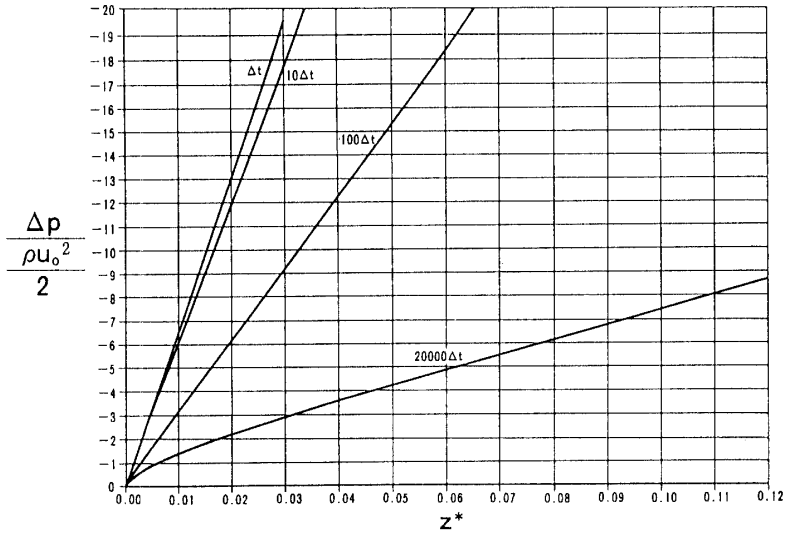

Fig. 12. Pressure Drop, Re=10000, on wall.

Table 3. Entrance length

Re	percent of fully developed value		Bibliography
	98%	99%	
1		0.33	Vrentas
10	0.0583	0.0681	*Kanda
50		0.047	Vrentas
60	0.045		Koyari
100	0.0437	0.0544	*Kanda
150		0.048	Vrentas
250		0.0535	Vrentas
2000	0.0440	0.0546	*Kanda
10000	0.0438	0.0555	*Kanda
		0.058	Langhaar

results of the numerical simulation at Reynolds number of 100. They agree well with one another in a steady state, time=8000*Δt. The numbers in Fig. 10 are Reynolds numbers of the experimental data.

3.4 Axial convective and viscous terms

The axial convective and viscous terms of two-dimensional Navier-Stokes equations are expressed in the cylindrical coordinates as follows,
Axial convective term:

$$v\frac{\partial u}{\partial r}+u\frac{\partial u}{\partial z} \tag{13}$$

Axial viscous term:

$$\frac{1}{\mathrm{Re}}\left(\frac{\partial^2 u}{\partial r^2}+\frac{1}{r}\frac{\partial u}{\partial r}+\frac{\partial^2 u}{\partial z^2}\right) \tag{14}$$

The flow characteristics in the entrance region can be seen clearly through the Figs. 13–15, which are the results of the numerical simulation at Reynolds number of 10000. The same pattern of Fig. 13 is seen for Reynolds numbers above 10. The axial convective term near the inlet is fairly larger than that of downstream, specially in central core $0<r<0.3$. Subscripts (1)–(6) are given in Figs. 14 and 15.

(1) The axial convective terms near the wall are nearly zero after $z^*>0.01$. The flow field near the wall develops fully within short distance from the inlet. This means that the pressure drop is the same as the value of the viscous term.

(2) and (3) The axial viscous term near the wall at $z^*=0.01$ is about -0.004 and the absolute value of it is almost the same as that of the convective term in the central core.

(4) The axial viscous terms near the edge, $z^*<0.01$, are about zero in the central core stream. In other words, since the radial pressure drop is uniform in the cross section, the acceleration force of fluid particles in the central core is the same as the value of the

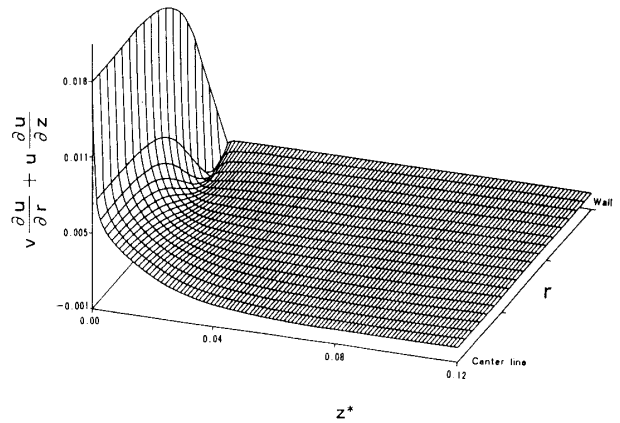

Fig. 13. Axial Convective Term (1), Re=10000.

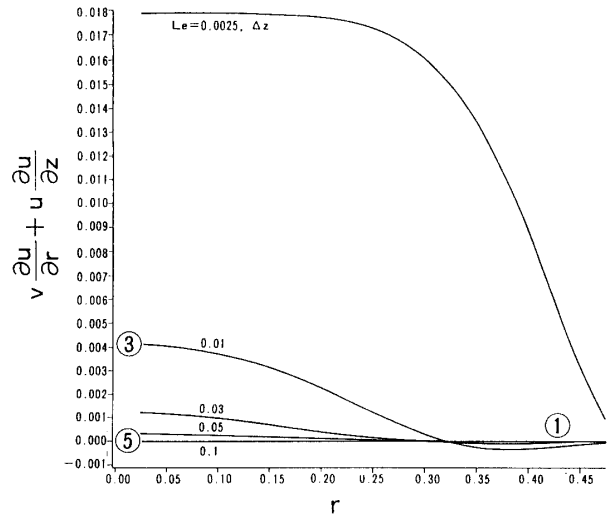

Fig. 14. Axial Convective Term (2), Re=10000.

viscous term near the wall. The condition for the boundary-layer equations is satisfied only in this short entrance region, $z^*<0.01$.

(5) The value of the axial convective term decreases with the distance from the inlet and becomes equal to zero in every cross-section after $z^*=0.1$. Zero means that the flow field is in a fuly developed state.

(6) The absolute value of the axial viscous term in the central core increases with the distance from the inlet and becomes equal to a constant, whic is the same as the value of the pressure drop.

Table 4 is the summary mentioned above.

3.5 Effect of disturbances upon velocty distribution

There can be assumed many kinds of disturbances which exercise a marked effect upon the transion from laminar to turbulent flow. Here, we simulated numerically a flow field in a case of 1.2 times singular stream function given only at $z=(0*\Delta z, 1*\Delta z)$ and $r=0.25$. We follow it whether the singularity of the velocity distribution will be

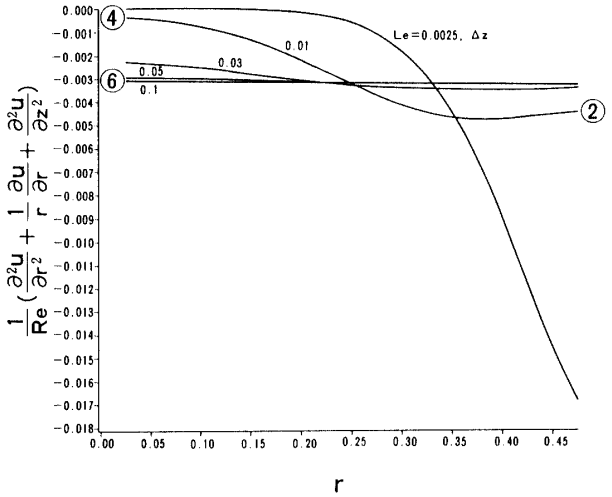

Fig. 15. Axial Viscous Term, Re=10000.

Table 4. Results (3) Values of Axial Convective and Viscous Terms

	before Lep		after Lep	
	near Wall	Central Core	near Wall	Central Core
Axial Convective Term	0 ①	$-\frac{\Delta p}{\Delta z}$ ③	uniform 0 ⑤	
Axial Viscous Term	uniform except inlet $\frac{\Delta p}{\Delta z}$ ②	0 ④	uniform $\frac{\Delta p}{\Delta z}$ ⑥	
Velocity Profile		uniform	parabolic	

amplified or will be damped as the time step develops. Figs. 16–18 are the results of the numerical simulation at Re=2000; Figs. 19–21 are the results at Re=10000. The singularity of the velocity distribution seems to be damped smoothly at Re=2000. The singularity at Re=10000 seems to be damped but a strong deformation of the velocity distribution at $z=2*\Delta z$ still remains.

3.6 Comparison with the N-S equations in a steady state

For steady two-dimensional flow, the velocity components in the tangential and radial directions are zero; the pressure is constant in every cross-section. The Navier-Stokes equations simplify to only one equation in the general dimensionless form:

$$\frac{dp}{dz^{**}} = \frac{2}{\mathrm{Re}}\left(\frac{d^2u}{dr^2} + \frac{2}{r}\frac{du}{dr}\right) \tag{15}$$

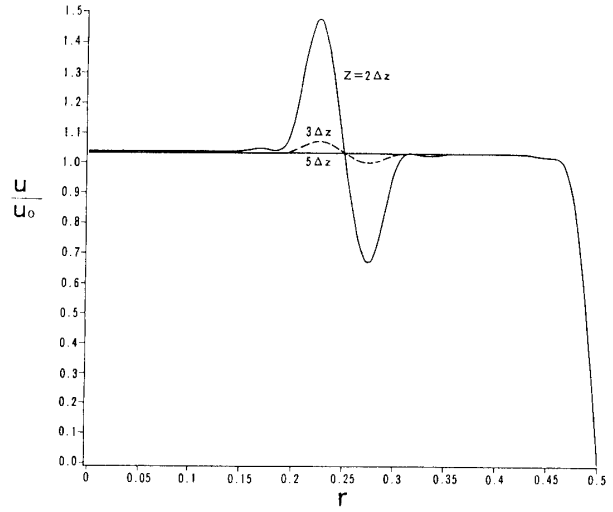

Fig. 16. Velocity Distribution with Disturbances, Re=2000, T=10*Δt.

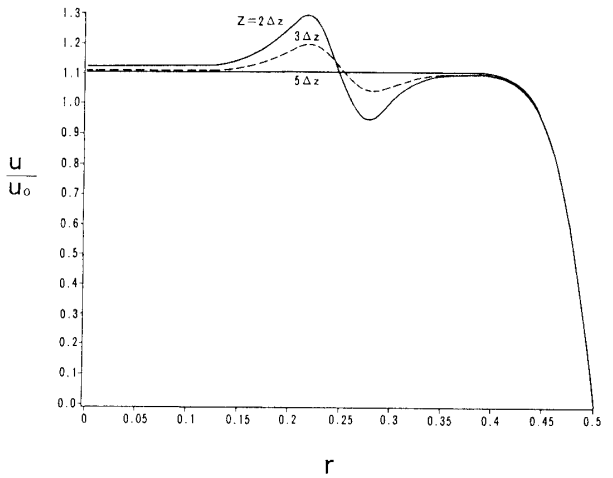

Fig. 17. Velocity Distribution with Disturbances, Re=2000, T=50*Δt.

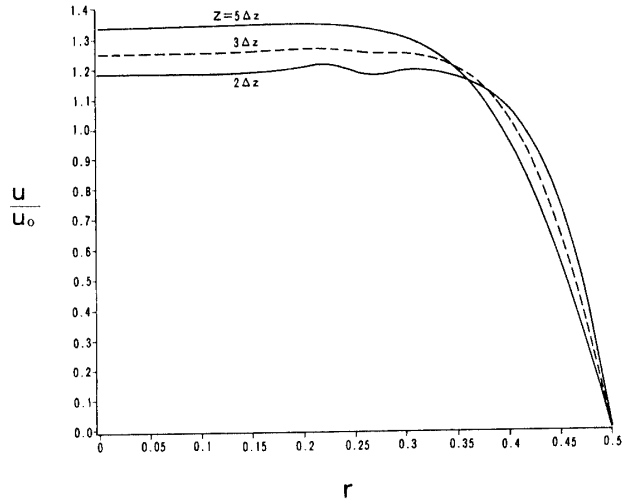

Fig. 18. Velocity Distribution with Disturbances, Re=2000, T=500*Δt.

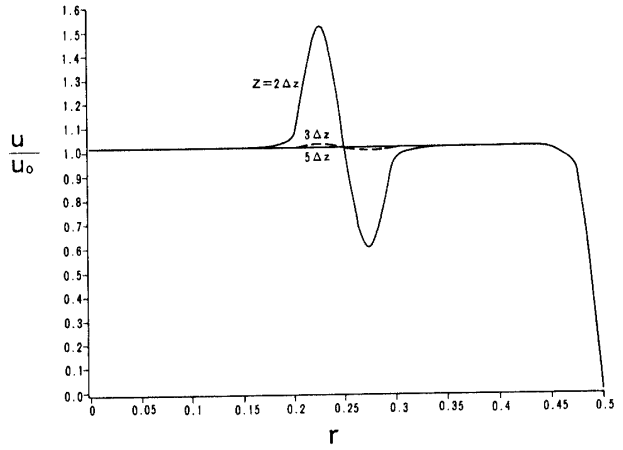

Fig. 19. Velocity Distribution with Disturbances, Re=10000, T=10*Δt.

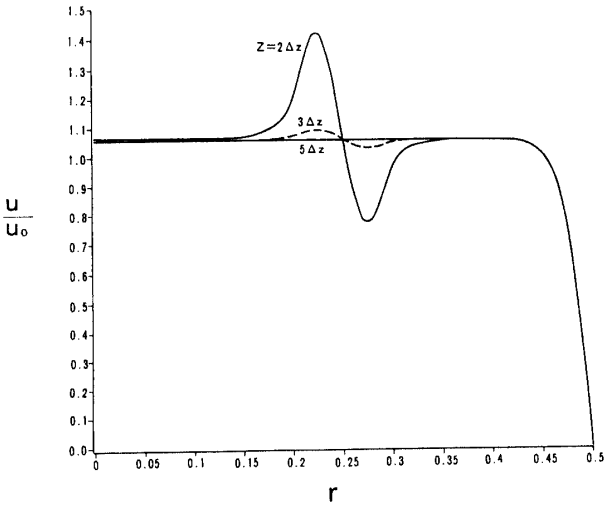

Fig. 20. Velocity Distribution with Disturbances, Re=10000, T=50*Δt.

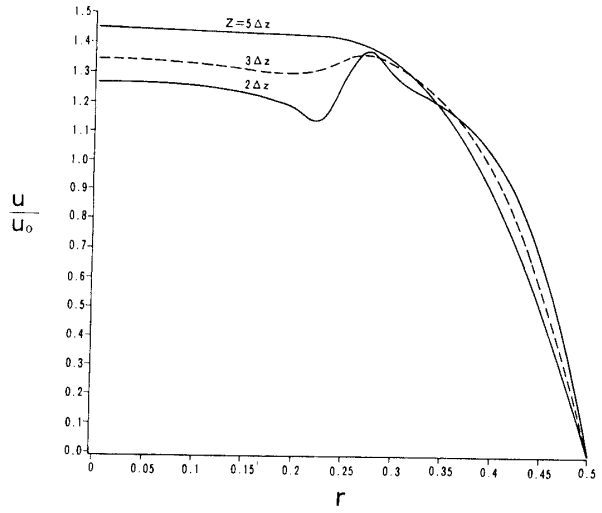

Fig. 21. Velocity Distribution with Disturbances, Re=10000, T=4500*Δt.

where $dz^{**}=dz/D$.

When the axial coordinate is made dimensionless by being divided by the Reynolds number, the equation is written as follows:

$$\frac{dp}{dz^*}=2\left(\frac{d^2u}{dr^2}+\frac{1}{r}\frac{du}{dr}\right) \tag{16}$$

where $dz^*=dz/(D\cdot\mathrm{Re})=dz^{**}/\mathrm{Re}$.

The velocity profile is the function of both of the radius and pressure drop, regardless of the Reynolds number.

Figs. 6–8 agree very well with one another and verify numerically that the development of the flow field of a circular pipe is same in the dimensionless coordinate z*=z/(D*Re) for Reynolds number more than 100.

§IV. Conclusion

An entrance model was presented in order to simulate numerically the flow characteristics such as velocity distribution, pressure drop, convective and viscous terms for four different Reynolds number of 10, 100, 2000, and 10000. The following results are obtained.

1) The aspect ratio of axial to radial space increments $\Delta z/\Delta r$, DZR, can be provided proportional to the Reynolds number below 10000 when variables have double precision in FORTRAN. For instance, the ratio is 1 at Re=10; 10 at Re=100, 100 at Re=2000 and 500 at 10000.

The results of the numerical computation in three cases of DZR=10, 50 and 100 are same one another for Reynolds number 2000.

2) Two-dimensional, time-dependent numerical solutions of the full Navier-Stokes equations exist smoothly even at more than the minimum critical Reynolds number under

the following conditions; (a) No disturbance is given. (b) Two 1.2 singular points of stream function exist constantly at $z=(0*\Delta z,\ 1*\Delta z)$ and $r=0.25$.

3) The dimensionless velocity distributions and pressure drops in the entrance region are nearly same for Reynolds numbers more than 100.

4) The dimensionless entrance length where the velocity distribution develops fully parabolic is 0.1 for Reynolds numbers more than 10.

The dimensionless entrance length for 98% and 99% velocity development are 0.045 and 0.055, respectively, for Reunolds number above 50.

5) The pressure drop is nearly same for Reynolds numbers above 100.

6) The condition which is satisfied for the boundary-layer theory is confirmed in the entrance region of $z^*<0.01$ from the results of the calculation of the axial convective and viscous terms.

References

[1] Schiller, L., ZAMM 2, 96–106 (1922).
[2] Langhaar, H. L.: Steady Flow in the Transition Length of a Straight Tube, J. Appl. Mechanics, *9*, A55–A58 (1942).
[3] Mohanty, A. K. and Asthana, S.B.L.: Laminar flow in the entrance region of a smooth pipe, J. Fluid Mech., *90*, 433–447 (1978).
[4] Perry, R. H. and Cilton, C. H.: Chemical Engineer's Handbook (5th edition), 5–34 (1983).
[5] Prandl, L. and Tietjens, O. G.: Applied Hydro- and Aeromechanics, Dover Publications, 1934.
[6] Schlichting, H.: Boundary-Layer Theory (7th edition), Mcgraw-Hill, 1978.
[7] Arakawa, M. and Matsunobu, Y.: Proceedings of the 17th Symposium on Turbulence, Japan Socienty of Fluid Mechanics, 1985.
[8] Oshima, K., Oshima, Y. and Ishii, Y.: Unannounced experimental data, 1985.
[9] Pearson, C. E.: A computational method for viscous flow problems, J. Fluid Mech., *21*, 611–622 (1965).
[10] Vrentras, J. S., Duda, J. L. and Bargeron, K. G.: Effect of Axial Diffusion of Vorticity on Flow Development in Circular Conduits: Part 1. Numerical Solution, A. I. Ch. E. J., *12*, 837 (1966).
[11] Koyari, Y.: Study of Unsteady Entrance Flow in Pipes (in Japanese), Ph. D. Thesis, Tokyo University, 1980.
[12] Kreith, E. and Eisenstadt, R.: Pressure Drop and Flow Characteristic of Short Capillary Tubes at Low Reynolds Numbers, Trans. ASME, *79*, 1070 (1957).